Superparamagnetic Gd- and Mn-substituted Magnetite Fluids Applied as MRI Contrast Agents

Jong Hee Kim,[†,a] Chang Hyun Lee,[‡] and Sang Kuk Lee[†,*]

[†]*Department of Chemistry, Pusan National University, Busan 609-735, Korea.* [*]*E-mail: sklee@pusan.ac.kr*
[‡]*Department of Diagnostic Radiology, Seoul National University Hospital, Seoul 110-744, Korea*
Received January 12, 2009, Accepted April 13, 2009

The experimental particle samples included $(Mn_{0.1}Fe_{0.9})O{\cdot}Fe_2O_3$ and $FeO{\cdot}(Gd_{0.1}Fe_{0.9})_2O_3$ with Mn^{2+} and Gd^{3+} substitutions in inverse spinel Fe_3O_4. A lecithin surfactant was adsorbed onto the magnetic particles by ultrasonication. The samples prepared showed excellent dispersibility at the mean size of 13 nm; their saturation magnetization values were 63 emu/g for the bare and Mn-substituted magnetites, and 56 emu/g for the Gd-substituted magnetite. The crystal structure of the substituted magnetites was very similar to that of the bare magnetite, due to a small amount of 0.1 mole fraction substituted in synthesizing the magnetite. The magnetite fluids, according to T2-weighted MR images, effectively diminished the signal intensity in the liver and spleen of Sprague-Dawley rats.

Key Words: Superparamagnetism, Magnetic nanoparticle, Imaging agent, *In vitro*, *In vivo*

Introduction

Magnetic oxide nanoparticles of the inverse spinel structure have attracted much attention owing to their interesting magnetic property and potential applications.[1,2] Although these nanoparticles have been studied often for the purposes of tumor diagnosis and treatment, there have been only a few studies on their utility as a magnetic resonance imaging (MRI) agent.[3,4] Such magnetic nanoparticles are fluidized with outlayered hydrophilic surfactants, and the resulting colloidal solution can be targeted within the body by means of the ligand markers on the nanoparticles[3] or be localized at a specific site under a magnetic or electromagnetic field.[5] The properties of those nanoparticles are mostly characteristic of superparamagnetism,[6] and are only slightly toxic to, but biocompatible with, a living body. Since in many cases of noninvasive MRI the imaging results are too vague to provide detailed diagnostic information, functionally versatile nanoparticles are now emerging as a promising candidate for a performance imaging agent. It is well-known that iron oxide magnetic nanoparticles enhance the MR signal when used as imaging agents for diagnosis. However, their signal sensitivity is still much lower compared with that obtained by fluorescence and positron emission tomography (PET).

In this work, magnetites were used as a source of iron oxide for a nanoparticle-based MR imaging agent. The chemical formulas of $(Mn_{0.1}Fe_{0.9})O{\cdot}Fe_2O_3$ for Mn^{2+} and $FeO{\cdot}(Gd_{0.1}Fe_{0.9})_2O_3$ for Gd^{3+} were conducted by an experimental composition of the magnetite which was substituted with Mn or Gd element. The metal ions of Mn and Gd have shown an excellent MR imaging effect except for their toxicity. In general, such materials become nontoxic by producing to a stable ion compound. The T1 and T2 values of MR for exact relaxivity were analyzed in detail with diluted concentrations of each imaging agent. Their imaging effects were also examined in *in vivo* test.

[a]Present address: Research Center for Advanced Magnetic Materials, Chungnam National University, Daejeon 305-764, Korea.

Experimental Details

Magnetic fluid preparation. Stoichiometric amounts of $FeCl_2{\cdot}4H_2O$ 1.72 g and $FeCl_3{\cdot}6H_2O$ 4.68 g for $Fe^{2+}/Fe^{3+}=0.5$, $FeCl_2{\cdot}4H_2O$ 1.55 g, $MnCl_2$ 0.11 g and $FeCl_3{\cdot}6H_2O$ 4.68 g for $(Mn^{2+}+Fe^{2+})/Fe^{3+}=0.5$ and $FeCl_2{\cdot}4H_2O$ 1.72 g, $GdCl_3{\cdot}6H_2O$ 0.64 g and $FeCl_3{\cdot}6H_2O$ 4.21 g for $Fe^{2+}/(Gd^{3+}+Fe^{3+})=0.5$ were dissolved in distilled water to synthesize nanoparticles of control sample Fe_3O_4, $(Mn_{0.1}Fe_{0.9})O{\cdot}Fe_2O_3$ and $FeO{\cdot}(Gd_{0.1}Fe_{0.9})_2O_3$, respectively. The mixed solution was heated to 80 °C under an Ar atmosphere. The pH value of the solution was adjusted to 10 by means of the rapid addition of ammonia water using a sonosmasher at 20 kHz and 140 W for 1 hr and then the precipitated black powder was washed until attaining a pH value of 8.[7] 80 mL of phosphate-buffered saline (PBS) was added to the washed precipitates, to which 2 mL of 20% (w/v) lecithin was added at 80 °C during ultrasonication of 1.5 hr. By cooling the fluid to room temperature, a stabilized colloid at the concentration of 33 mg/mL was obtained. This process is shown in brief in Figure 1. Mn^{2+} and Gd^{3+} were substituted for the corresponding Fe ions, with only a 0.1 mole fraction in the magnetite compound which was satisfactory within the soluble limit. The particle size and the lattice parameter were observed by transmission electron microscopy (TEM) and X-ray diffraction (XRD), respectively, and the saturation magnetization was measured within a field range of ± 10 kOe using a vibrating sample magnetometer.

***In vitro* and *in vivo* MR imaging.** The Mn- and Gd-substituted magnetite contrast fluids, including the control sample of Fe_3O_4, were diluted in test tubes for different concentrations. MR imaging of phantoms was performed with a standard wrist coil using a 1.5T MR imager (Excite HD; GE Medical Systems, Milwaukee, WI) to obtain T2-axial images. The sequence parameters were repetition time = 5,000 ms, effective echo time = 90 ms, view field = 120×120 mm, flip angle = 90°, matrix = 256×160, slice thickness = 2.0 mm, slice separation = 0 mm, and excitation number = 3.0.

The T2 values were measured using conventional spin-echo

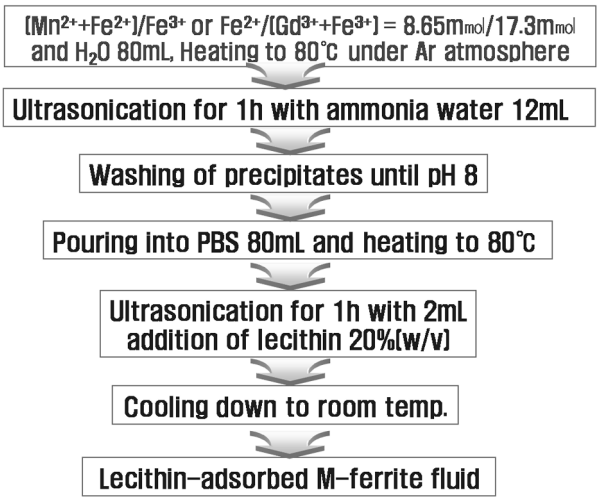

Figure 1. Sonochemical process for preparation of Mn- and Gd-substituted magnetite fluids.

(TR/TE = 2000 ms/10, 15, 20, 25, 30, 40, 50, 60 and 70 ms) and gradient-echo sequences (TR/TE = 1000 ms/4, 11, 18, 25, 32, and 39 ms) with one echo for each sequence while varying the TE, and were calculated by fitting the signal intensities diminished with increasing TEs into a mono-exponential function. The T1 values were measured using inversion-recovery fast spin-echo sequences (TR/TE/TI = 2200/18/50, 100, 200, 500, 800, 1200 and 2100 ms) while varying the TI and keeping the TR and TE constants. Since the image intensities of various TIs were proportional to $| [1-(1-k)\exp(-TI/T1)]M_o |$, the T1 was determined using a least squares fit of the image intensities in this equation.[8]

The T2-weighted coronal images, using a Fast Imaging Employing Steady-State Acquisition (FIESTA) pulse sequence (TR/TE 10.1/3.9, slice thickness = 2 mm, slice gap = 2 mm, matrix = 256×190, excitation number = 2) were obtained by applying each contrast magnetite fluid to Sprague-Dawley rats weighing 300 g to 400 g. The contrast fluids were injected into the tail vein at the dose of 33 mgFe/kg.

A quantitative analysis was performed by means of a signal intensity measurement, in both test tubes and the liver and spleen of rats. For the purposes of an *in vitro* test, the signal intensity was measured in the center of the test tubes containing different doses of the contrast magnetite fluids, using a defined region of interest (ROI) on the T1- and T2-weighted images. The ROI size was as small as 0.22 mm^2. Also, an *in vivo* test was performed on a liver parenchyma. The signal intensity of the lesion in the hepatic parenchyma was measured using the defined ROI for the T1- and $T2^*$-weighted images whose size was 4.43 mm^2.

Results and Discussion

Particle properties. A natural surfactant, lecithin is a phospholipid, in which the ionic part of the phosphorus and nitrogen atoms is hydrophilic and the non-ionic part of the alkyl groups is hydrophobic. Since lecithin has an excellent chemical affinity, the fluid of hydrophilic particles can be prepared by a simple one-step adsorption process. The magnetite nanoparticles could be 87% homogeneously dispersed by adding 20% (w/v) lecithin.[9]

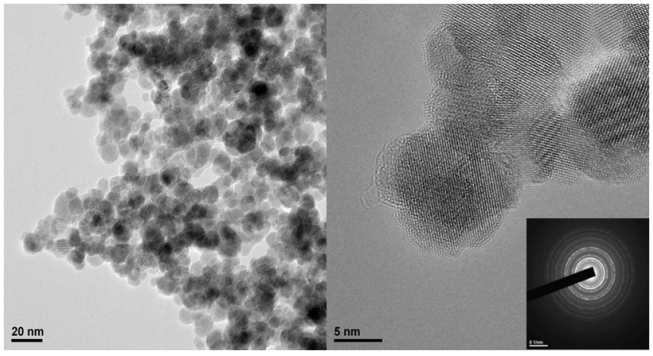

Figure 2. TEM image of typical magnetite particles fluidized by adsorption of lecithin 20% (w/v). The small insert image on the lower right indicates the selected area's electron diffraction pattern.

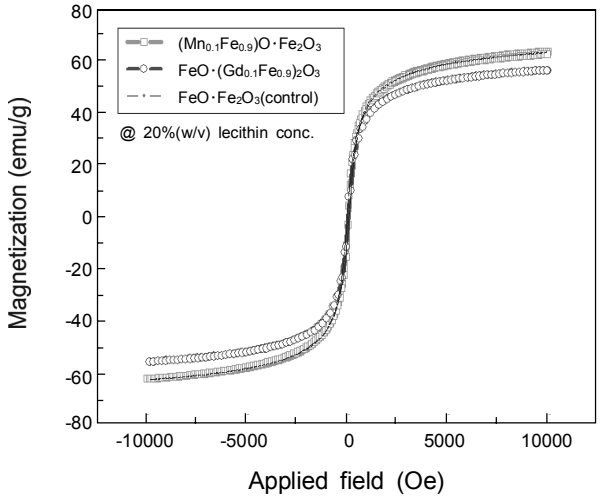

Figure 3. Magnetization curves of lecithin-adsorbed nanoparticles for bare magnetite Fe_3O_4, Mn-substituted magnetite $(Mn_{0.1}Fe_{0.9})O\cdot Fe_2O_3$ and Gd-substituted magnetite $FeO\cdot(Gd_{0.1}Fe_{0.9})_2O_3$.

Figure 2 shows that the magnetic particles are spherical with a mean size of 13.0 nm and possessing high crystallinity. The 1hr ultrasonic irradiation at 20 kHz used in the process of synthesis usually results in small particle sizes within a narrow size distribution.[4] As shown in Figure 3, saturation magnetization values of the bare magnetite Fe_3O_4, Mn-substituted magnetite $(Mn_{0.1}Fe_{0.9})O\cdot Fe_2O_3$ and Gd-substituted magnetite $FeO\cdot(Gd_{0.1}Fe_{0.9})_2O_3$ were 62.7 emu/g, 62.6 emu/g and 55.8 emu/g, respectively, at the 20% (w/v) concentration of lecithin surfactant. The saturation magnetization for the bare magnetite and the Mn-substituted magnetite was practically the same due to a large magnetic moment of the ions (Mn^{2+}: 5, Fe^{2+}: 4), whereas the magnetization values of the Gd-substituted magnetite were slightly decreased by a lower amount of the bare magnetite due to the added paramagnetic Gd^{3+} component. The prepared nanoparticles also were superparamagnetic, with no remnant magnetization. In general, oxide magnetic particles behave superparamagnetically at sizes above 5 nm and tend to appear paramagnetic at 19 nm,[10] and

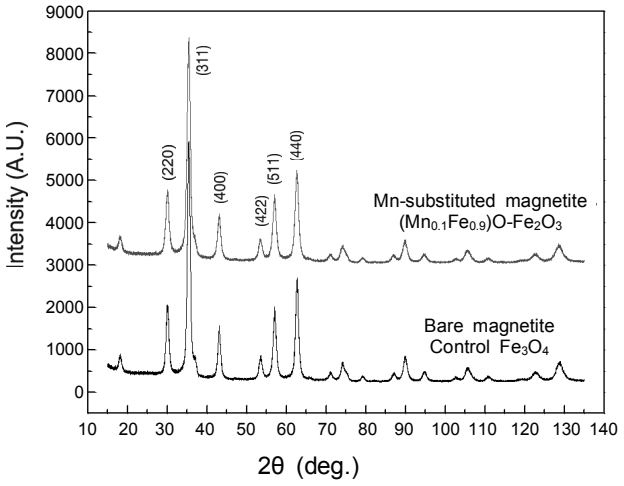

Figure 4. X-ray diffraction patterns for nanoparticles of Mn-substituted magnetite $(Mn_{0.1}Fe_{0.9})O{\cdot}Fe_2O_3$ and bare magnetite Fe_3O_4.

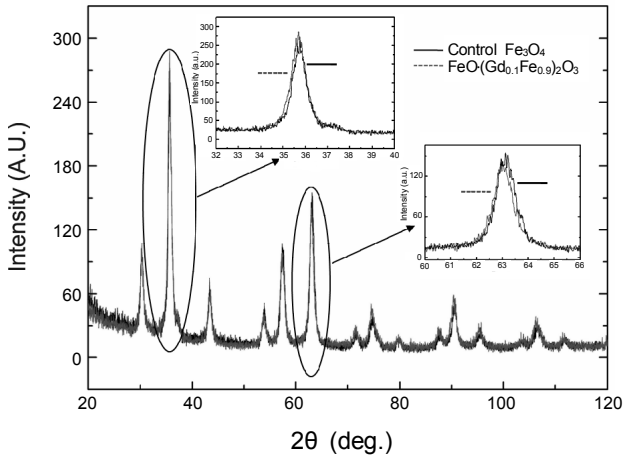

Figure 5. Comparison of peak positions in high-resolution powder diffraction patterns for nanoparticles of Gd-substituted magnetite $FeO{\cdot}(Gd_{0.1}Fe_{0.9})_2O_3$ and bare magnetite Fe_3O_4.

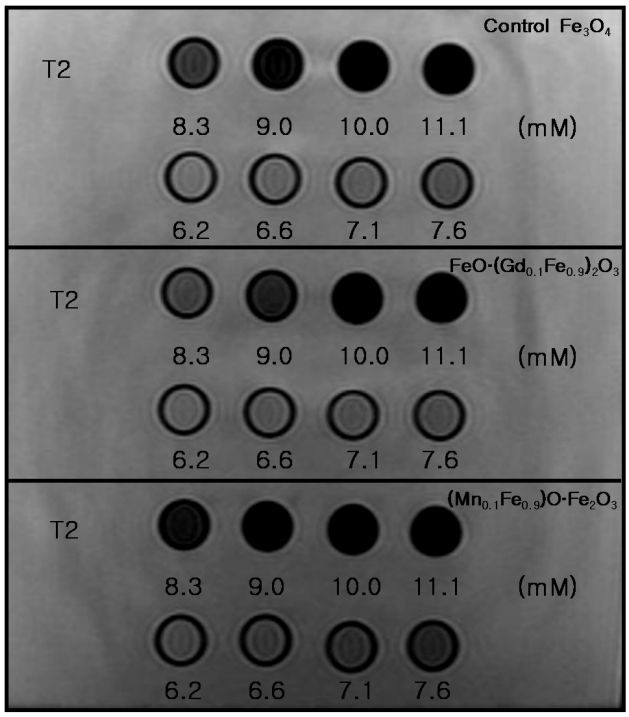

Figure 6. T2-weighted MR images of phantoms at various concentrations with different contrast magnetite fluids. The MR signal intensity begins to be differential at 8.3 mmol/mL. The Mn-substituted magnetite shows the darkest signal intensity among the three kinds of magnetites in the T2-weighted images, whereas the Gd-substituted magnetite exhibits stronger signal intensity than does the control bare magnetite.

Table 1. T1, T2 and $T2^*$ values measured in phantoms for 8.3 mmol/mL contrast magnetite fluids

fluid classification	T1	T2	$T2^*$ (msec)
control Fe_3O_4	1316.5 ± 12	94.6 ± 5	89 ± 2
$FeO{\cdot}(Gd_{0.1}Fe_{0.9})_2O_3$	1602.0 ± 20	113.5 ± 4	109 ± 2
$(Mn_{0.1}Fe_{0.9})O{\cdot}Fe_2O_3$	990.3 ± 32	79.4 ± 7	80 ± 2

the magnetization values decrease with increasing lecithin concentrations because the organic lecithin layer reduces the total magnetic moment of nanoparticles per unit weight.[9] Figure 4 shows XRD patterns of the prepared fluid particles. The analysis results revealed that lattice parameter, 0.8378 nm for the Mn-substituted magnetite was much the same as that (0.8373 nm) of the bare magnetite in the Fe_3O_4 phase. This similarity in crystal structure could be caused by a very small amount of substitution added with 0.1 mole fraction. Two-valence cation of Mn is almost perfectly substituent in the magnetite crystal, owing to the similar ionic radius (Fe^{2+}: 0.074 nm, Mn^{2+}: 0.080 nm) as well as the same cubic type of element structure. Also, magnetites have been substituted by Co, Ni, Cu and Ca elements with the same valence to investigate saturation magnetization, metal composition and lattice parameter.[7,11] However, in the case of the substitution of three-valence cation, the difference between the ionic radii of Fe (0.064 nm) and Gd (0.102 nm) is significant. Moreover, the Fe structure is different from that of Gd element with a hexagonal type. Figure 5 shows high-resolution powder diffraction patterns taken at Pohang Light Source 8C2 Beam Line for the nanoparticles of the bare magnetite and the Gd-substituted magnetite. The peaks of the Gd-substituted magnetite were slightly shifted to a low angle from the bare magnetite's peak position. In general, such an angle shift is caused by increase of the lattice parameter with the substitution of larger ion. However, in order to obtain exact substitution efficiency for these elements, a supplementary analysis needs to be carried out with a continuous increase of substituted elements using Raman spectroscope or electron probe micro analyzer.

MRI characterization. In Figure 6, the phantoms are arranged in the T2-weighted MR images according to the different fluid concentrations. The contrast magnetite fluids revealed a difference in signal intensity in T2WI at the diluted concentration of 8.3 mmol/mL. Table 1 lists the T1, T2, and $T2^*$ values measured in the phantoms for each 8.3 mmol/mL contrast magnetite fluid. The Mn-substituted magnetite exhibited the strongest susceptibility effect, whereas the Gd-sub-

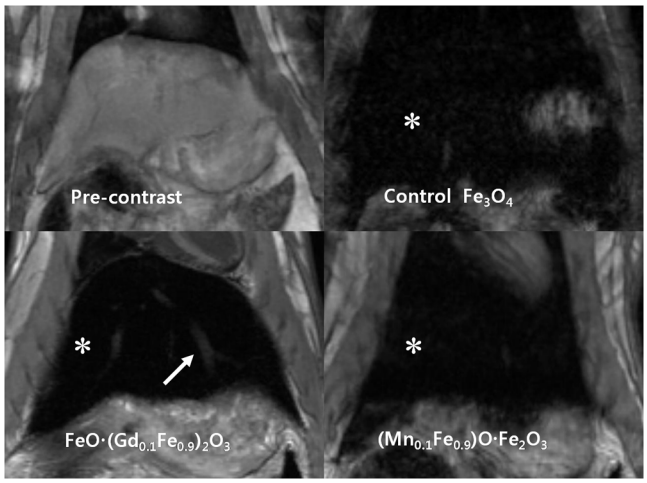

Figure 7. T2-weighted coronal MR images by different contrast magnetite fluids in liver of a rat. The Hepatic parenchymal signal intensity, in the pre-contrast T2-weighted image, is diminished with injection of all of the magnetite fluids. Note the effect of the Gd-substituted magnetite, showing the characteristics of both T1 (portal vein enhancement, white arrow) and T2 (dark signal intensity of hepatic parenchyma, symbol *) contrast agents.

stituted magnetite increased the signal intensity rather than the bare magnetite. In all of the cases, a mono-exponential diminishment of the signal intensity allowed for a very unambiguous determination of the T2 and $T2^*$ values.

Figure 7 shows that although there were few differences of the hepatic parenchymal signal intensity among the injected contrast fluids in the T2-weighted images, the signal intensity was clearly diminished with the application of the three kinds of magnetite fluids. Thereby do the contrast magnetite fluids allow for the T2 contrast effect in the liver and spleen. The Gd-substituted magnetite also produced a T1 contrast effect, through the paramagnetic property of gadolinium, in addition to the T2 effect. This kind of contrast agent can be expected to be useful for the purpose of better visualizing hepatocellular carcinoma or other pathologic entities by means of the enhancement of lesions in T1-weighted images and suppression of the background liver signal intensity in T2-weighted images.

Conclusions

Lecithin-adsorbed $M_xFe_{3-x}O_4$ (M: Mn and Gd) fluids were prepared from substituted magnetite nanoparticles by the sonochemical method. The shape of the prepared fluid particles was spherical, the mean particle size was 13.0 nm, and their saturation magnetizations were 63 emu/g for the bare magnetite Fe_3O_4 and the Mn-substituted magnetite $(Mn_{0.1}Fe_{0.9})O{\cdot}Fe_2O_3$, and 56 emu/g for the Gd-substituted magnetite $FeO{\cdot}(Gd_{0.1}Fe_{0.9})_2O_3$. The crystal structure of the Mn-substituted or Gdsubstituted magnetite was much the same as that of the bare magnetite, probably owing to a very small amount of 0.1 mole fraction having been substituted. These magnetite fluids showed the characteristics of T2 MR contrast agents, having diminished the signal intensity of the liver and spleen when tested in Sprague-Dawley rats. Therefore, the substituted magnetite fluids potentially can be used in medical diagnostic procedures.

Acknowledgments. This study was financially supported by Pusan National University in program, Post-Doc. 2008.

References

1. Li, X.; Kutal, C. *J. Magn. Magn. Mater.* **1994**, *134*, 249.
2. Betancourt-Galindo, R.; Ayala-Valenzuela, O. *J. Magn. Magn. Mater.* **2005**, *294*, e23.
3. Lee, J.-H.; Huh, Y.-M.; Jun, Y.-W.; Seo, J.-W.; Jang, J.-T.; Song, H.-T.; Kim, S.; Cho, E.-J.; Yoon, H.-G.; Suh, J.-S.; Cheon, J. *Nature Medicine*, *Technical Reports* (Advance Online Publication), 24 Dec. **2006**, 1-5.
4. Lee, H.; Shao, H.; Huang, Y.; Kwak, B. K. *IEEE Transactions on Magnetics* **2005**, *41*, 4102.
5. Senyei, A.; Widder, K.; Czerlinski, C. *J. Appl. Phys.* **1978**, *49*, 3578.
6. Silva, J. B.; De Brito, W.; Mohallem, N. D. S. *Mater. Sci. Eng.* B **2004**, *112*, 182.
7. Park, S. I.; Lim, J. H.; Hwang, Y. H.; Kim, J. H.; Kim, C. G.; Kim, C. O. *Physica Status Solidi* (a) **2007**, *204*, 3913.
8. Zhu, D. C.; Penn, R. D. *Magn. Reson. Med.* **2005**, *54*, 725.
9. Park, S. I.; Kim, J. H.; Lim, J. H.; Kim, C. O. *Curr. App. Phys.* **2008**, *8*, 706.
10. Lee, S. W.; Woo, K. J.; Kim, C. S. *J. Magnetics* **2004**, *9*, 83.
11. Park, S. I.; Vinh, L. K.; Kim, J. H.; Kim, C. O. *J. Magn. Magn. Mater.* **2006**, *304*, e409.